Astron. Astrophys. 228, 331–340 (1990)

ASTRONOMY AND ASTROPHYSICS

^{12}CO ($J=2-1$) mapping of M82

N. Loiseau [1,5], N. Nakai [2], Y. Sofue [3], R. Wielebinski [1], H.-P. Reuter [1], and U. Klein [4]

[1] Max-Planck-Institut für Radioastronomie, Auf dem Hügel 69, D-5300 Bonn 1, Federal Republic of Germany
[2] Nobeyama Radio Observatory, Minamimaki, Minamisaku, Nagano 384-13, Japan
[3] Institute of Astronomy, University of Tokyo, Mitaka, Tokyo 181, Japan
[4] Radioastronomisches Institut der Universität Bonn, Auf dem Hügel 71, D-5300 Bonn 1, Federal Republic of Germany
[5] Instituto de Pesquisas Espaciais, INPE-DAS, C.P. 515, 12201 São José dos Campos, S.P., Brazil

Received April 3, accepted July 21, 1989

Abstract. The ^{12}CO ($J=2-1$) emission of M 82 was mapped with an angular resolution of 13″. The data have been compared with the ^{12}CO ($J=1-0$) observations of M 82 with a 16″ beam made in the same area. A clear ring of CO is seen rotating around the centre of M 82. Differences in the ($J=2-1$) to ($J=1-0$) intensity ratios are interpreted as variations in the optical depth and/or excitation temperature. Based on the CO data we find that the gas rotates more slowly in the halo than in the disk of M 82.

Key words: carbon monoxide – galaxies – halo of galaxies – molecular gas – star burst

1. Introduction

The peculiar galaxy M 82 (NGC 3034; 3 C 231; Arp 337) has been studied in all spectral ranges, from radio to X-rays. It was classified as IrrII (Holmberg, 1950; Sandage, 1961) or IO (de Vaucouleurs and de Vaucouleurs, 1964) but also regarded as a disk galaxy seen nearly edge-on (Lynds and Sandage, 1963). The distance is estimated to be 3.25 Mpc (Tammann and Sandage, 1968). Unusual Hα filaments are seen extending out of the galactic disk up to 3 kpc along the minor axis. These filaments were first studied by Lynds and Sandage (1963) who concluded that there is a massive gas outflow from the nucleus. In fact at this time the suggestion was made that M 82 is an exploding or colliding galaxy (e.g. Burbidge et al., 1964; Axon and Taylor, 1978). Recently Bland and Tully (1988) made Fabry-Perot observations in the Hα and [N II] λ 6583 lines and found two components: filamentary narrow line emission arising from the surfaces of two bubbles originating from a bipolar outflow, and broad-line and continuum emission arising from a faint halo that rotates with the disk. Such an extension towards the halo, suggesting an outflow, is more clearly seen in the thermal X-ray emission (Watson et al., 1984; Kronberg et al., 1985). Optical polarization observations (Visvanathan and Sandage, 1972; Bingham et al., 1976; Schmidt et al., 1976) indicated the presence of scattering dust up to 2 kpc above the plane of the galaxy.

Studies of the extended radio continuum emission at several frequencies were made by Seaquist et al. (1985). Recent studies of the radio continuum flux of M 82 (Klein et al., 1988) have revealed that only 15% of the total emission at 32 GHz is thermal. Observations of the nuclear area at 86 GHz by Carlstrom (1988) showed that the spectrum is flatter near 86 GHz, which could either indicate thermal emission (free-free or dust) at higher frequencies or could also indicate (like in our Galaxy) peculiar flat-spectrum nonthermal emission (Reich et al., 1988). Equipartition considerations suggest a magnetic field strength of $\sim 50\,\mu$G which is one order of magnitude stronger than that of usual spiral galaxies.

The large infrared luminosities observed in the central regions of many galaxies (e.g. Telesco and Harper, 1980) are often interpreted to be the result of bursts of star formation (e.g. Rieke et al., 1980). IRAS observations have confirmed M 82 to be one of the most luminous FIR sources (e.g. Wunderlich et al., 1987). Young superclusters of stars (Kronberg et al., 1972; O'Connell and Mangano, 1978) and more than 40 compact radio sources, most of which could be superluminous, young supernova remnants (Kronberg et al., 1985), have been discovered in the nuclear region. While star bursts seem to provide a plausible explanation for the extreme luminosity, the triggering of such star bursts and the way the gas is supplied are not yet obvious. Possibly the star burst can be triggered by the tidal interaction with its neighbour galaxy M 81. Indications for this interaction are the H I bridge observed by Cottrell (1977) and by Gottesman and Weliachew (1977), and the existence of non-circular motions in the outer regions of M 82.

H I and OH studies by Weliachew et al. (1984) showed that the molecular gas is concentrated in a rotating ring of radius 250 pc. The OH masers that were detected are seen to lie inside the rotating ring.

It is not surprising in view of its luminosity at various frequencies that M 82 was one of the first galaxies detected in CO (Rickard et al., 1975; Solomon and deZafra, 1975). Sutton et al. (1983) observed the ^{12}CO ($J=2-1$) transition and found the line intensities to be 2–3 times higher than those of the ^{12}CO ($J=1-0$) line. This fact suggests that the lines are optically thin in the nuclear region of M 82. Young and Scoville (1984) and Stark and Carlson (1984) covered an $8' \times 5'$ field and detected CO gas extending up to 2 kpc out of the plane. Olofsson and Rydbeck (1984) showed that the ^{12}CO ($J=1-0$) gas has an elongated structure along the major axis. Recent CO observations give us higher angular resolution in the ^{12}CO ($J=1-0$) (Nakai et al., 1987; Lo et al., 1987; Carlstrom, 1988), ^{12}CO ($J=2-1$) (Loiseau et al., 1988a), and in the ^{13}CO ($J=2-1$) (Loiseau et al., 1988b) lines (see also the review by Sofue, 1988).

Send offprint requests to: R. Wielebinski

In this paper we present details of the ^{12}CO ($J=2-1$) observations (Sect. 2) and intercompare all the existing data (Sect. 3). Based on this study we discuss the physical conditions of the molecular gas in the central region of M 82 (Sect. 4).

2. Observations

The ^{12}CO ($J=2-1$) rotational transition line at 230.538 GHz was mapped in the central region of M 82 using the IRAM 30-m telescope. The observations were made in November 1986 in the course of test observations at 230 GHz with a cooled Schottky barrier diode receiver. The receiver had a noise temperature of $T_{\rm rec}$ (DSB) $\sim$360 K, and the system SSB noise temperature including the atmospheric losses was 1400 to 1900 K. The half-power beam width was 13″ corresponding to 205 pc. The antenna beam, aperture, forward scattering and spillover efficiencies were 0.45, 0.27, and 0.86, respectively. The backend was a filter bank spectrometer of 512 channels $\times$1 MHz, giving a velocity resolution of 1.3 km s^{-1}.

A grid of 102 points was observed covering the central 1′.6 × 1′.0, or 1.6 kpc × 1.0 kpc centred on the 2.2 μm emission peak (Rieke et al., 1980) at RA = 9^{h}51^{m}43^{s}.9, DEC = 69°55′01″ (epoch 1950.0). The major axis was taken to be PA = 65° (Nilson, 1973). The inner 1′.0 × 0′.6 was observed with a grid spacing of 6″, and the outer region with a 12″ grid interval.

Pointing calibration was done with the continuum source 0716+714 which is 13° distant from M 82 and typically at the same elevation. Due to the low intensity of this source at 230 GHz, the pointing measurements were done with the SIS receiver at 90 GHz in the DSB mode, showing pointing errors of less than 2″ rms. The two beams are parallel within an accuracy of $\sim$3″ rms, indicating that, although the repeatability was very good, the absolute pointing error can be expected to be less than 4″ rms.

The position switching technique was used with 30 s integration time per on-position. The observations were repeated in order to average up to 10 min integration time per on-position for most of the points. Typical rms noise values of the spectra are of the order of $T_R^*=0.1$ K (antenna temperature corrected for atmospheric, ohmic, and spillover losses). The off-position was chosen 10′ to the east of the centre along the major axis. The spectra were centred on $V_{\rm LSR}=220$ km s^{-1} so that the spectrometer covered a velocity range from -112 to 553 km s^{-1}.

In addition to ^{12}CO (2−1) we have observed ^{12}CO (1−0) at the three central points along the major axis with a grid spacing of 6″. At the ^{12}CO ($J=1-0$) frequency, the HPBW was 23″ (362 pc), and the main beam, forward scattering and spillover efficiencies were 0.55 and 0.78, respectively. The observing equipment and procedures were the same as for ^{12}CO (2−1).

3. Results

3.1. Spectra

The observed spectra are shown in Fig. 1. The grid is in X–Y coordinates with the X axis aligned with the major axis of the galaxy (P.A. = 65°). The spectra were smoothed to a velocity resolution of 2.6 km s^{-1}. The indicated intensity scale is in units of T_R^*.

The shapes of these high signal-to-noise profiles show remarkable differences from point to point. The profiles are complex, exhibiting more than one velocity component in most of the points. The main component of the profiles is obviously associated with the rotating molecular ring already observed in other lines such as in H I absorption (Weliachew et al., 1984) and in the ^{12}CO ($J=1-0$) line (Nakai et al., 1987). The line profile at the centre ($X=0'.0$, $Y=0'.0$) is clearly asymmetric with respect to the systemic velocity of the galaxy (220 km s^{-1}), and the antenna temperature at $V_{\rm LSR}\simeq 250$–300 km s^{-1} is much higher than that at $V_{\rm LSR}\simeq 150$–200 km s^{-1}. Moreover the antenna temperature at $X=0'.1$ is higher than that at $X=-0'.1$. On the other hand, spectra of ^{12}CO ($J=1-0$) do not show such an asymmetry (Olofsson and Rydbeck, 1984; Nakai et al., 1987). This is attributed to the variation of optical depth with velocity (see Sect. 4.1).

Also striking is the presence of a strong blue-shifted component in the SE region of the galaxy and a red-shifted component in

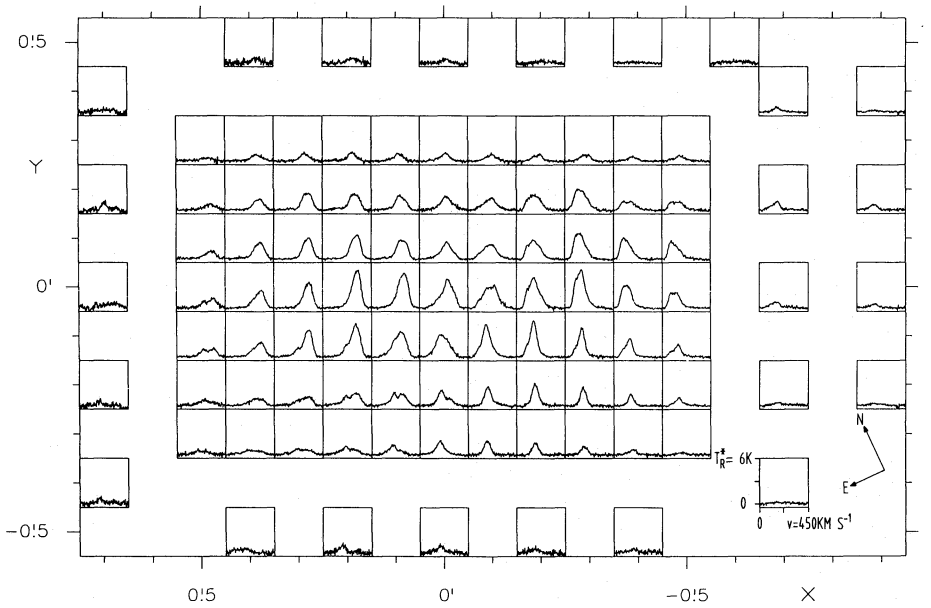

Fig. 1. Observed spectra of the ^{12}CO ($J=2-1$) line of the galaxy M 82, smoothed to 2.6 km s^{-1} velocity resolution

the NW region, both extending far outside the plane. Other components can be distinguished although not easily separated. At least some of these components are due to the outflow of gas from the disk (Sect. 4.1). The combination of all these components yields very wide profiles, with widths of up to almost 400 km s^{-1}, especially in the central and SE regions. The width of the central profiles is consistent with the model of Rickard et al. (1977) which assumes a ring rotating at 70 km s^{-1}, expanding away from the nucleus at 50 km s^{-1}, and having a velocity dispersion of 60 km s^{-1} within the ring. The very broad eastern profiles are due to the mixing along the line of sight of the disk component and that flowing out from the disk (Sects. 3.1 and 4.1).

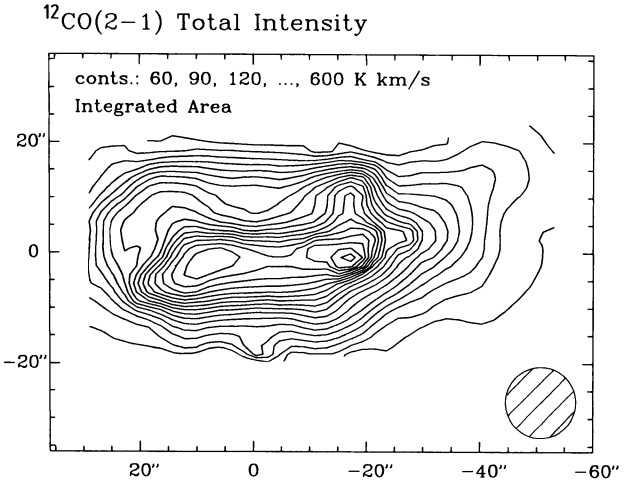

Fig. 2. Distribution of the integrated intensity of the ^{12}CO ($J=2-1$) line, $I_{CO}=\int T_R^* \, dv$ (in K km s^{-1})

3.2. *Intensity distributions*

Figure 2 shows the integrated intensity distribution of the ^{12}CO ($J=2-1$) transition line, $I \equiv \int T_R^* \, dv$. Figure 3 is the superposition of the intensity map on a near-IR photograph. The map again shows clearly the two peaks associated with the molecular ring. The separation between the two peaks is slightly smaller in our map than in the higher resolution maps (e.g. Weliachew et al., 1984; Lo et al., 1987), due to our larger beam width. This effect is even more pronounced in the ^{12}CO ($J=1-0$) map of Nakai et al. (1987) (HPBW = 16″), where the peaks appear at about half the distance of the H I absorption peaks. We therefore adopt the ring dimensions given by Weliachew et al. (1984) with a mean radius of about 250 pc and width of about 170 pc.

The rotating ring characteristics may be better seen in the channel maps in Figure 4 which are presented at 20 km s^{-1} intervals. The highest intensities are observed in the channel maps at $V_{LSR}=140$–160 km s^{-1} and 300–320 km s^{-1}, with the peak positions at $X=-0'.3$ and $+0'.2$, or -300 pc and $+200$ pc, respectively.

In Figs. 2 and 4 spur-like extensions can be seen towards higher latitudes which were already detected in other lines. The spurs centred at $X=-0'.3$, $Y=0'.2$ and at $X=0'.0$, $Y=-0'.3$ are also indicated in the ^{13}CO (2−1) map of Loiseau et al. (1988b), and in the ^{12}CO (1−0) map of Lo et al. (1987). The extended feature in the NW region is coincident with the one observed in the ^{12}CO ($J=1-0$) (Nakai et al., 1987; Lo et al., 1987). The enhancement at $X=-0'.45$, $Y=0'.05$ is also seen in the high-resolution continuum map by Kronberg et al. (1985). The eastern spurs are also observed in the ^{13}CO (2−1) map (Loiseau et al., 1988b).

The distribution of these spurs suggesting two hollow structures extending above and below the galactic plane, with their "walls" inclined by $-30°$ with respect to the plane of the galaxy.

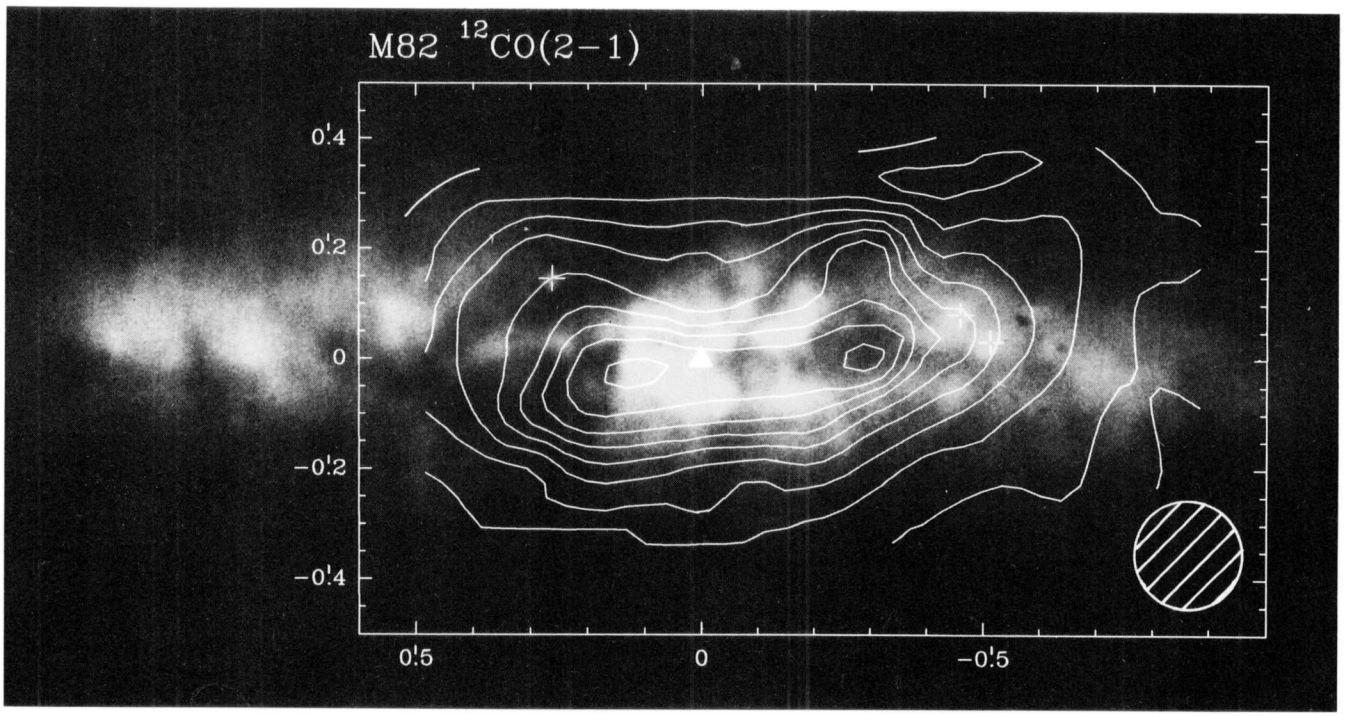

Fig. 3. Superposition of the intensity map onto a near-IR photograph of M82 (courtesy by F. Bertola). The filled triangle marks the assumed centre of the galaxy at $\alpha_{50}=9^h51^m53^s.9$, $\delta_{50}=69°55'01''$ (Rieke et al., 1980). The observations have been done relative to the major axis of M82, assuming a position angle of 65°

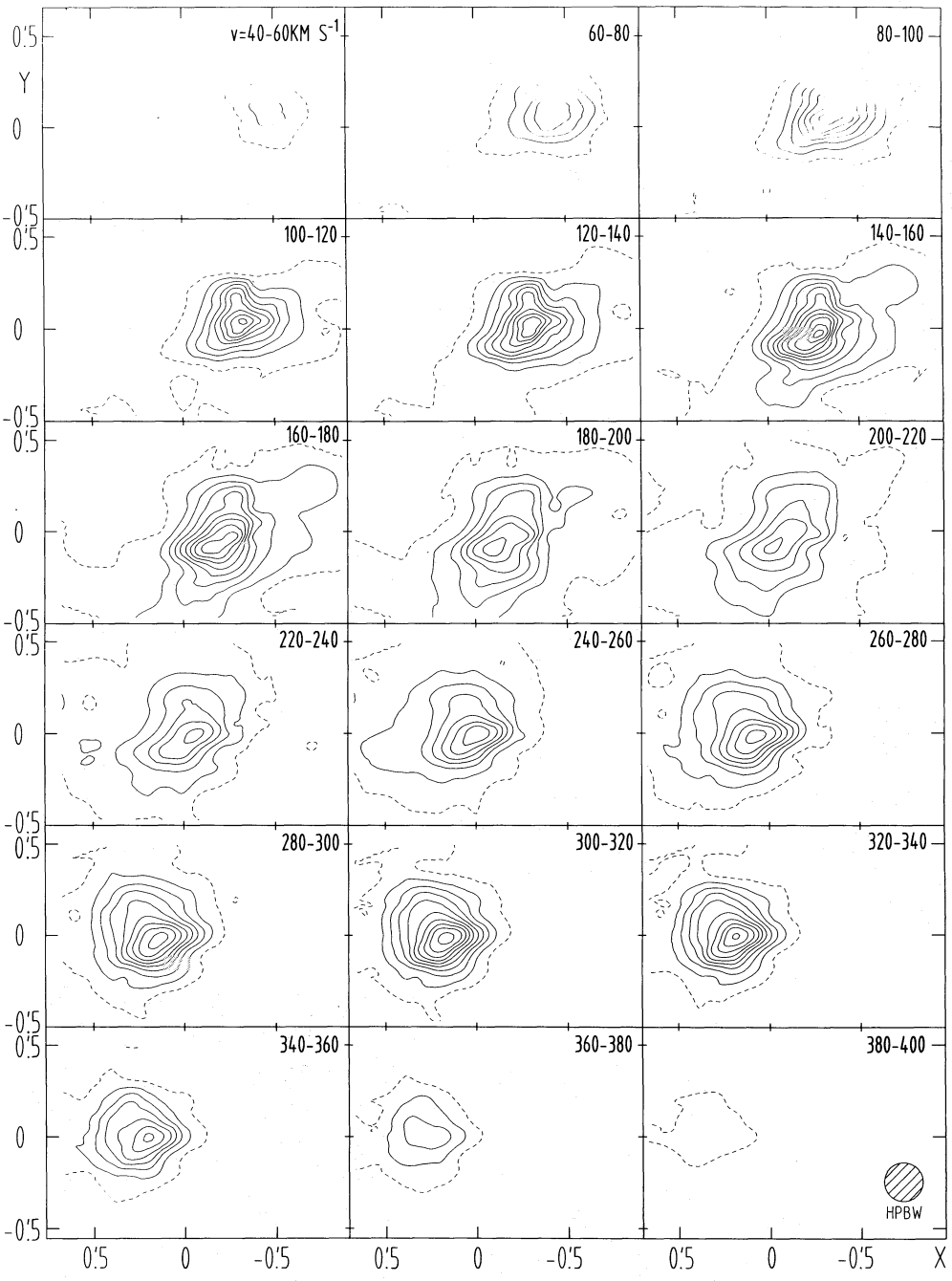

Fig. 4. Channel maps of the ^{12}CO ($J=2-1$) line intensity at every 20 km s^{-1} velocity interval. Contours are 5 (dashed), 15, 25, ... K km s^{-1}

It may also be noted that a third clump near the centre, at $X\sim -3''$, $Y=0''$, has been found in the ^{13}CO ($J=2-1$) intensity map (Loiseau et al., 1988b), which is coincident with an enhancement found on higher-resolution ^{12}CO ($J=1-0$) maps (Lo et al., 1987; Carlstrom, 1988), SNR distribution (Kronberg et al., 1985) and H I and OH absorption maps (Weliachew et al., 1984). This central clump is not resolved in the present map, but there is an indication of an enhancement of the ^{12}CO ($J=2-1$) intensity towards this direction.

3.3. Velocity distribution

The kinematical centre of the rotating ring can be estimated as the middle point between the maximum and minimum velocity. In this case the components of the profiles produced by the rotating ring should be separated from the contributions of the outflowing gas. The separation of the profiles into such components proved to be very uncertain, but the position of the peaks can be determined from the channel maps (Fig. 4) and the position-velocity diagrams (Figs. 5 and 6). The position of the maximum velocity peak was estimated from the $V_{LSR}=300-320$ km s^{-1} map, and that of the minimum velocity peak from the $V_{LSR}=140$–160 km s^{-1} map. The position obtained for the kinematical centre is given in Table 1. The positions for the kinematical centre estimated from H I absorption and optical data are also given in Table 1 for comparison.

The systemic velocity of the ring can be estimated as the mean between the peaks of the maximum and minimum velocity. We get

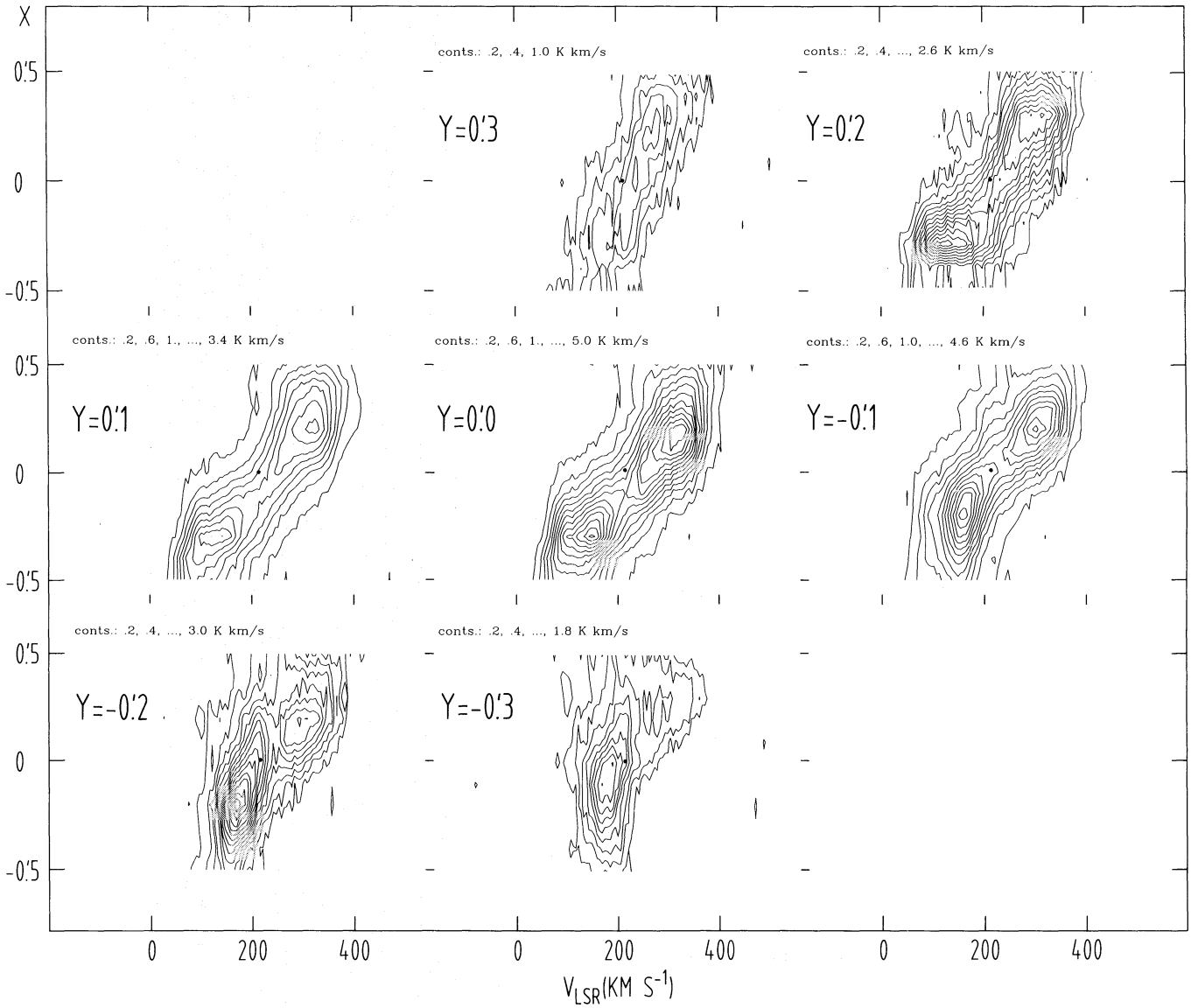

Fig. 5. Position (X)-velocity maps taken parallel to the major axis at every 0'.1 interval of Y

$V_{LSR} = 230 \pm 10\,\mathrm{km\,s^{-1}}$ which is comparable with the value of $225 \pm 10\,\mathrm{km\,s^{-1}}$ found by Weliachew et al. (1984). The maximum rotation velocity of the ring would then be $V_{rot} \sim 80\,\mathrm{km\,s^{-1}}$.

The distribution of the different velocity components can be derived from the position-velocity diagrams (Fig. 5) taken parallel to the major axis. In Fig. 7 we plot the mean velocity against distance from the centre along the major axis (crosses). We also plot the peak velocity (filled circles). The two curves show significant differences in the inner region. This is because the peak velocity represents better the inner rotation characteristics, while the mean velocity is more or less a superposition of contributions from gas components in different places where the velocity changes rapidly.

In Fig. 8 we display the velocity field derived from the present ^{12}CO (2−1) observations, along with the velocity fields of the ^{12}CO (1−0) line obtained by Nakai et al. (1987) and the ^{13}CO (2−1) line as observed by Loiseau et al. (1988b). In addition to the rotation of the disk and ring, the ^{12}CO (2−1) velocity field exhibits an inclination of the iso-velocity contours near the minor axis. Such an inclination was also observed in the ^{12}CO (1−0) line (see Fig. 8), and is confirmed in the channel maps at $V_{LSR} = 200-220\,\mathrm{km\,s^{-1}}$ and 220–240 km s^{-1}, with a significant tilt with respect to the vertical line (see Fig. 4).

Nakai et al. (1987) have attributed this inclination to an outflow of gas perpendicular to the disk at a velocity of 200–300 km s^{-1}. The outflow velocity can be also measured in our position-velocity maps along the minor axis. The maps at $X = -0'.3$ to $+0'.4$ in Fig. 6 show a high-latitude component as well as a disk component. The high-latitude component has a velocity gradient of $dv/dY \simeq 80\,\mathrm{km\,s^{-1}}$/arc min within $Y = \pm 0'.4$, indicating $\sim 32\,\mathrm{km\,s^{-1}}$ at $Y = \pm 0'.4$. This velocity corresponds to a vertical flow velocity of $\sim 230\,\mathrm{km\,s^{-1}}$, assuming an inclination of $\sim 82°$ (Lynds and Sandage, 1963), consistent with the above value. A similar tilt of the velocity field has been observed in the Hα line (Heckathorn, 1972). Nakai et al. (1987) attributed the outflow to mass ejection by the central star burst activity (Rieke et al., 1980). They have estimated the energy required to accelerate the out-of-plane gas to the observed velocity to be some 10^{55} erg.

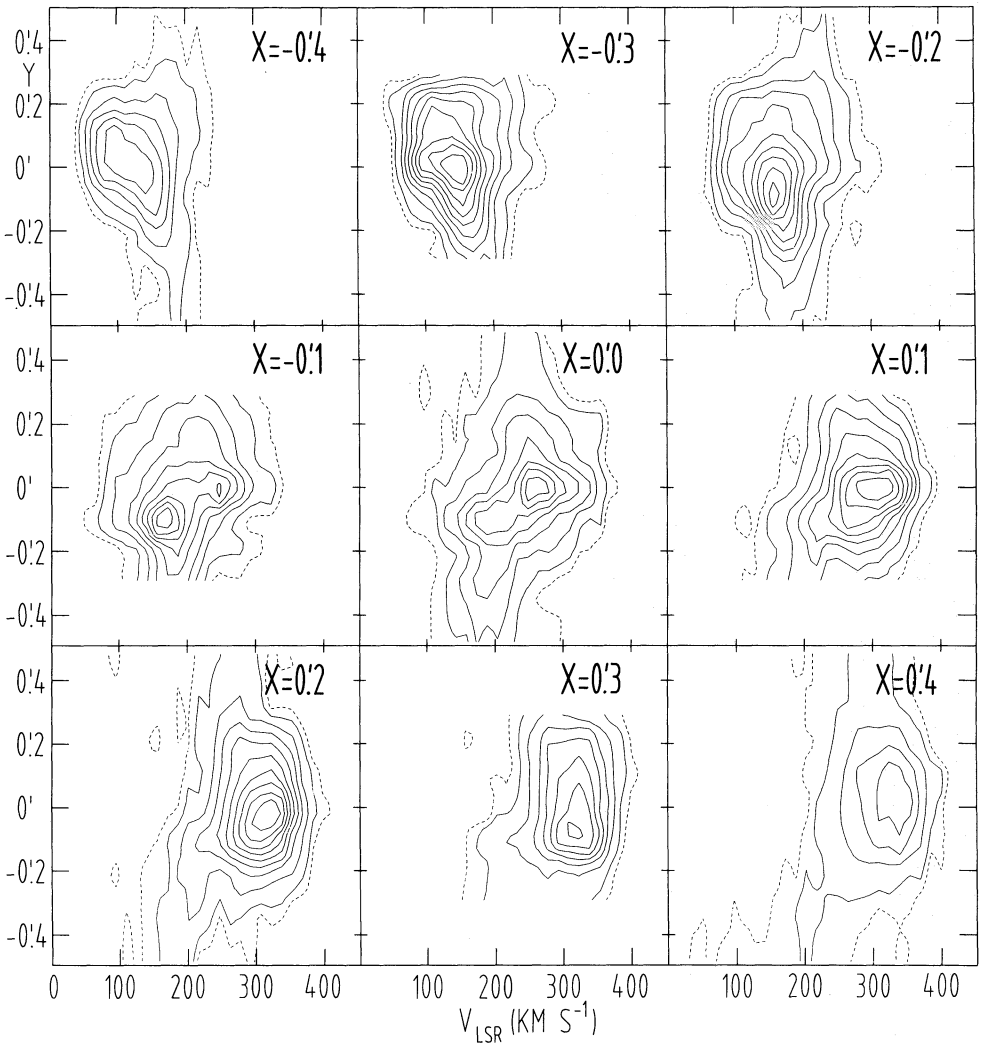

Fig. 6. Position (Y)-velocity maps across the major axis drawn at every 0'.1 interval of X. Contours are 0 (dashed), 0.5, 1.0, 1.5, 2.0, ... K

Table 1. Kinematical centre of the rotating ring and the 2.2 μm emission peak position

	α_{1950}	δ_{1950}
H I absorption [a]	$9^h51^m43^s.2 \pm 0^s.4$	$69°55'00''.1 \pm 1''.5$
Optical [b]	$9^h51^m43^s.6 \pm 0^s.3$	$69°54'58''.5 \pm 1''.5$
2.2 μm emission peak [c]	$9^h51^m43^s.9$	$69°55'01''$
^{12}CO (2−1) [d]	$9^h51^m43^s.4 \pm 0^s.2$	$69°54'58''.3 \pm 3''.6$

[a] Weliachew et al. (1984)
[b] O'Connell and Mangano (1978)
[c] Rieke et al. (1980)
[d] Present paper

As already pointed out by Loiseau et al. (1988b) the ^{13}CO velocity field shows a good alignment of contours along the minor axis, suggesting normal rotation. The discrepancy between the velocity field obtained from the ^{13}CO and that from ^{12}CO may be due to the fact that the ^{13}CO emission is so weak that the observed line profiles of ^{13}CO are not deep enough to detect the gas far out of the disk plane.

Figure 8 also shows V_{LSR} [^{12}CO (2−1)] > V_{LSR} [^{12}CO (1−0)] > V_{LSR} [^{13}CO (2−1)] at the centre. This results because the optical depth τ at $V_{LSR} \simeq 100$–$150\,\mathrm{km\,s^{-1}}$ is larger, increasing the antenna temperature of ^{13}CO (2−1), while τ is smaller at 200–300 km s^{-1}, increasing the temperature of ^{12}CO ($J = 2-1$).

4. Discussion

4.1. The line ratios

If we assume LTE, or if the excitation temperatures for the $J = 1-0$ and $2-1$ transitions are the same, the ratio r of brightness temperatures, T_b, of a cloud for the two transitions can be expressed by

$$r = T_b(2-1)/T_b(1-0) = [1 - e^{-\tau_{21}}]/[1 - e^{-\tau_{10}}], \quad (1)$$

where τ_{21} and τ_{10} are the optical depths of the corresponding transitions. The ratio of the optical depths between 2−1 and 1−0 is given by

$$\tau_{21}/\tau_{10} = 2\,\{[1 - e^{-h\nu_{21}/kT_{ex}}]/[1 - e^{-h\nu_{10}/kT_{ex}}]\} \cdot e^{-h\nu_{10}/kT_{ex}}, \quad (2)$$

where h is Planck's constant, k Boltzman's constant, T_{ex} the excitation temperature, and ν_{21} and ν_{10} are the frequencies of the 2−1 and 1−0 transitions, respectively.

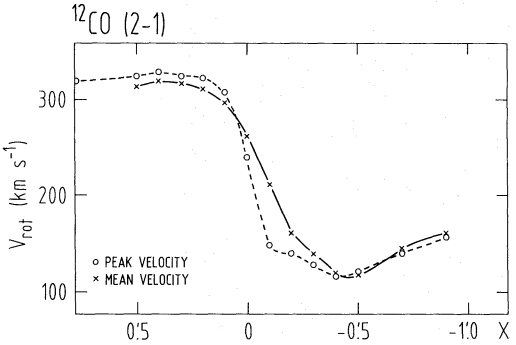

Fig. 7. The rotation curve of M 82 obtained from the mean velocities of ^{12}CO (2−1) line (crosses) and from the peak velocities (circles)

In the extreme case of $\tau_{21}, \tau_{10} \gg 1$ (optically thick) Eq. (1) can be approximated by $r \simeq 1$. For the other extreme case of τ_{21}, $\tau_{10} \ll 1$ (optically thin), we have $r \simeq \tau_{21}/\tau_{10}$, and for $h\nu < kT_{ex}$,

$$r \simeq 4\, e^{-5.53/T_{ex}}. \quad (3)$$

If we assume that $T_{ex} \simeq T_{dust} \simeq 45$ K (Telesco and Harper, 1980), we have $r \simeq 3.5$, while if the temperature is lower, say for example $T_{ex} \sim 20$ K (as in galactic clouds), we have $r \sim 3$.

In Fig. 9a we compare the spectra of the (2−1) and (1−0) transitions for the central three positions, smoothed to the same angular resolution of 23″ in units of T_R^*. Figure 9b shows the ratios of the main beam brightness temperature, $T_{mb} = T_R^* \cdot \eta_{fss}/\eta_{mb}$ between the various CO transitions, where the main beam efficiencies η_{mb} are 0.56 and 0.45 at 115 and 230 GHz, respectively. The ratios of the ^{12}CO ($J = 2-1$) and ^{12}CO ($J = 1-0$) line intensities are $r \sim 2$ at $V_{LSR} < 200$ km s^{-1} and $r \simeq 2.5$–3 at $V_{LSR} > 200$ km s^{-1}. The optical depths τ_{21} and τ_{10} can be estimated by assuming the excitation temperature T_{ex}. The lower limit of T_{ex} is given by the brightness temperature T_b of the CO emission.

Interferometer observations of ^{12}CO ($J = 1-0$) have given a peak brightness temperature T_b of 9–15 K with 7″ resolution (Lo et al., 1987) and 15 K for 5″ resolution (Carlstrom, 1988), so that the excitation temperature is estimated by $T_{ex} > T_b + T_{bg} \simeq 12-18$ K, where T_{bg} is the cosmic background radiation temperature (3 K). Actually, the value of T_{ex}, which is required to achieve the high value of $r \sim 2-3$, should be higher than 20 K for an LTE condition. The upper limit of T_{ex} is given by the colour temperature of the dust emission, $T_{dust} \sim 45$ K (e.g. Telesco and Harper, 1980). From Eqs. (1) and (2), the optical depth τ_{10} corresponding to $r = 2$ is obtained as ∼0.40 and 0.53 at $T_{ex} = 20$ K and 40 K, respectively, corresponding to optical depths τ_{21} of 1.1 and 1.7. For $r = 2.5$, $\tau_{10} \simeq 0.08$ and 0.26 and $\tau_{21} \simeq 0.21$ and 0.85 for $T_{ex} = 20$ K and 45 K, respectively.

The small optical depths are supported by the large ratios of brightness temperatures between ^{12}CO and ^{13}CO in Fig. 9b. The ratios of ^{12}CO (1−0)/^{13}CO (1−0) and ^{12}CO (2−1)/^{13}CO (2−1) are 15–20 at $V_{LSR} > 200$ km s^{-1}, and are well above the value of ∼5 for typical giant molecular clouds in our Galaxy (Solomon et al., 1979). This fact is consistent with an optically thin CO gas. Since the beam averaged column density $N_{CO} \sim 10^{17}$–10^{18} cm^{-2} (Sect. 4.2) is not lower than that of a giant molecular cloud in our Galaxy, the small optical depth may be caused by a high excitation temperature and a large velocity dispersion produced by vigorous star formation in the central region of M 82.

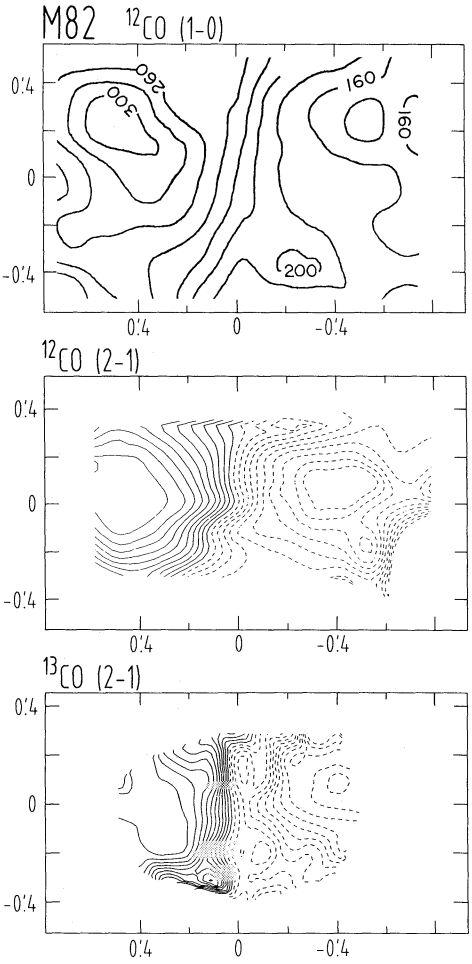

Fig. 8. The median velocity fields obtained (a) for the ^{12}CO (1−0) line (Nakai et al., 1987); (b) for the ^{12}CO (2−1) line (present observations), and (c) for the ^{13}CO (2−1) line (Loiseau et al., 1988b). For the (2−1) observations the negative contours are shown dashed, the first solid (zero) contour represents the assumed systematic velocity of 220 km s^{-1}. The velocity interval is 10 km s^{-1}

As pointed out by Knapp et al. (1980) and Olofsson and Rydbeck (1984) the small optical depths would be discrepant with an effective production of CO and H_2. Also the detection of HCN and HCO+ $J = 1-0$ emissions by Stark and Wolff (1979) point to high densities. On the other hand, the optical image of M 82 indicates that the extinction is quite nonuniform. Thus the bright ^{12}CO lines would originate in a relatively small amount of material arranged in small clumps or thin shells so that the mean column density in molecules is small while the beam filling factor is fairly large. Recent submillimetre measurements suggest a filling factor of about 0.1 (Lugten et al., 1986).

Since the line profiles do not change drastically for the two transitions, ^{12}CO ($J = 2-1$) and ^{12}CO ($J = 1-0$), we may approximate the mean ratio of the brightness temperature by the ratio of integrated intensities, $I(2-1)/I(1-0)$. Using this fact we can produce a map of the distribution of the line intensity ratio in the observed area. This is displayed in Fig. 10a. As is readily seen from the figure the ratio is larger near the galactic plane, and attains a maximum towards the centre and the molecular ring, where we have $r = T_{mb}(2-1)/T_{mb}(1-0) \sim I(2-1)/I(1-0) \sim 2.5$. On the other hand, the ratio is nearly equal to unity outside the disk, at $|Y| > 0'.2$ (200 pc).

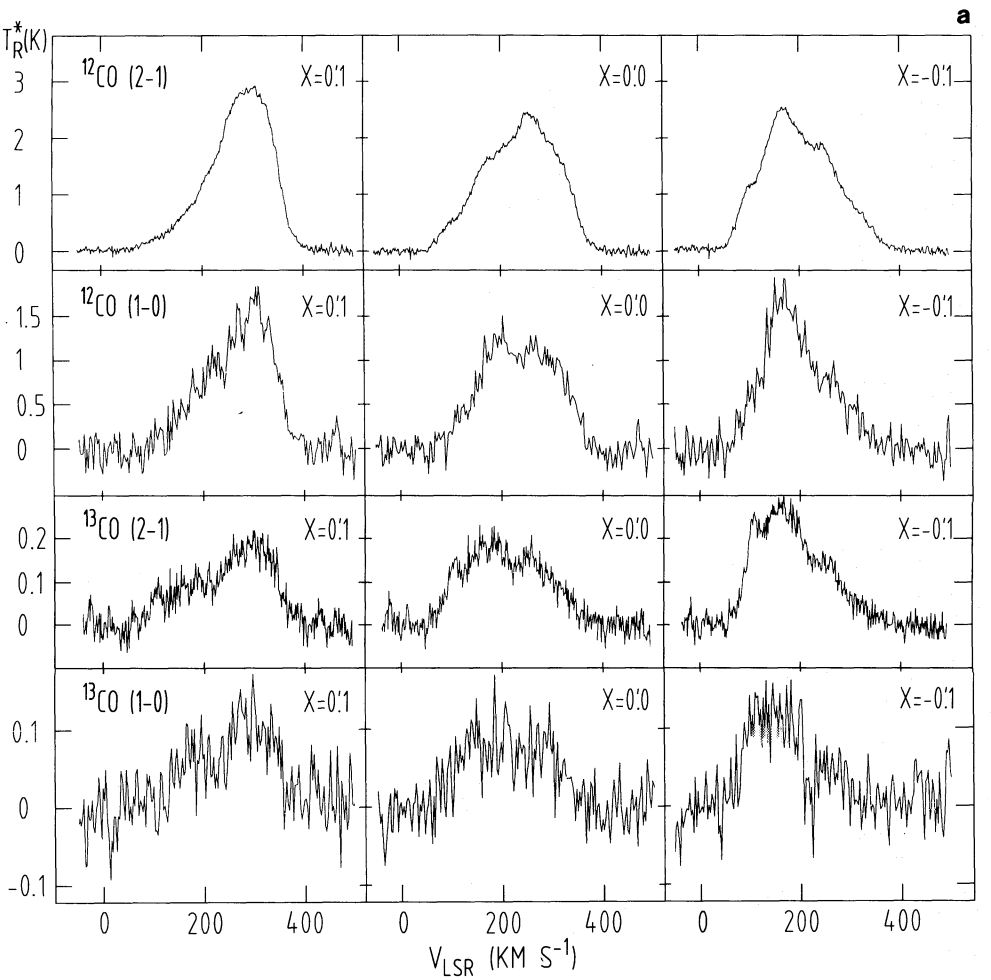

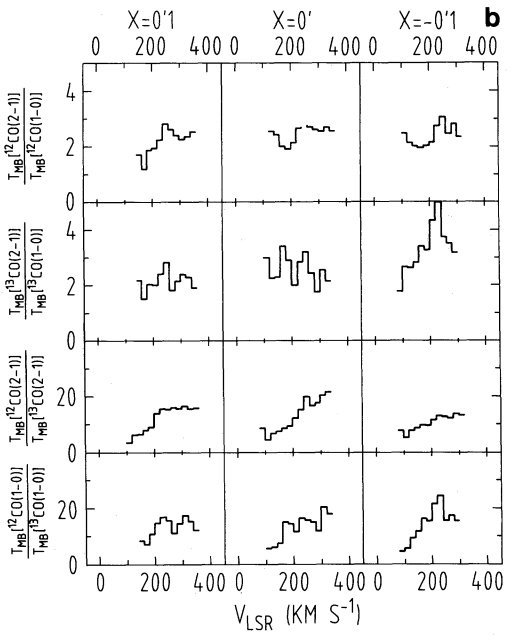

Fig. 9. a Spectra of the ^{12}CO (2−1), ^{12}CO (1−0), ^{13}CO (2−1), and ^{13}CO (1−0) lines for the central region of M 82, obtained with the IRAM 30-m telescope smoothed to the same angular resolution of 23″. **b** Ratios of the lines as a function of the velocity

Figure 10b shows the distribution of the intensity ratio $I(^{12}CO)/I(^{13}CO)$ for the 2−1 transitions, where the ^{13}CO data were taken from Loiseau et al. (1988b). Comparing Fig. 10b with 10a, it turns out that the ^{12}CO (2−1)/^{13}CO (2−1) ratio on the major axis (along the disk) is nearly inversely proportional to the ratio of 2−1 and 1−0 line intensities. This means that the excitation temperature varies along the disk as well as the ^{12}C/^{13}C abundance ratio.

Outside the galactic plane, the ratio of $I(^{12}CO)/I(^{13}CO)$ increases to more than 20 within the molecular spur (Fig. 2) except at $(X, Y) \simeq (-17'', +10'')$, while the ratio $I(2-1)/I(1-0)$ decreases to 1–1.5 which is consistent with smaller optical depths τ_{21} and τ_{10} and lower ^{13}CO abundance. The low $I(2-1)/I(1-0)$ line ratio for an optically thin gas suggests a low excitation temperature of $T_{ex} < 10$ K. This may be reasonable for gas in the halo of M 82, as the gas flowing out of the central region spreads over the halo so that the density of molecular hydrogen decreases there. The low density and very large outflow velocity of 200–300 km s^{-1} may result in a decrease of excitation temperature even if the kinetic temperature is high (i.e. non-LTE condition).

The ratio of 10 to 20 of the integrated intensity, $I(^{12}CO)/I(^{13}CO)$, in Figure 10b yields a lower limit to the abundance ratio [^{12}CO]/[^{13}CO] averaged along the line of sight for the same excitation temperature, since τ is around unity for the ^{12}CO ($J = 2-1$) line, while for ^{13}CO (1−0) the optical depth is smaller. To deduce the abundance ratio from the optical depths, detailed knowledge about the excitation conditions and about the line-of-sight structure of the molecular gas is necessary.

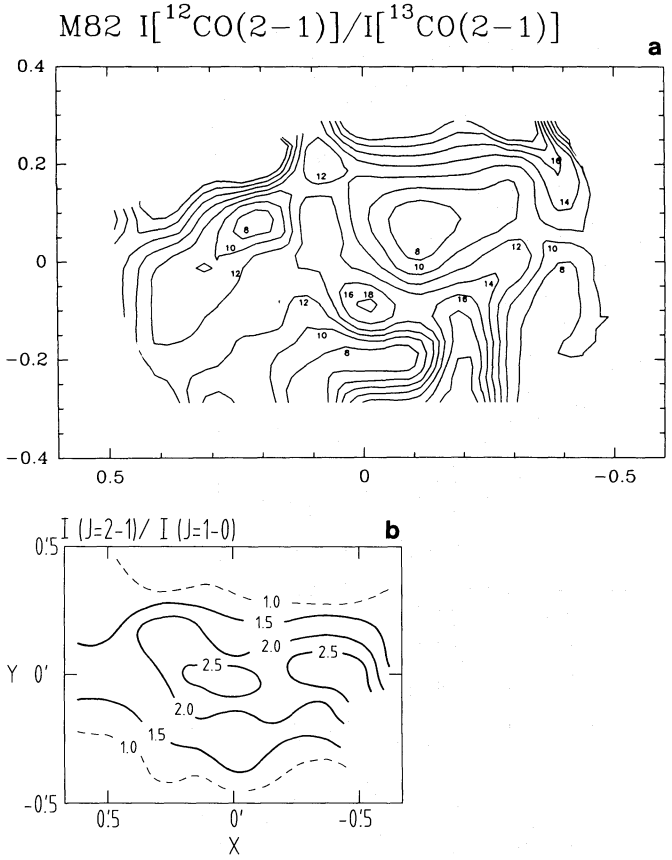

Fig. 10. **a** Distribution of the ratio of the integrated intensity of the ^{12}CO (2−1) line to that of the (1−0) line constructed after smoothing to the same angular resolution of 16″. **b** Ratio of the ^{12}CO (2−1) and ^{13}CO (2−1) line intensities

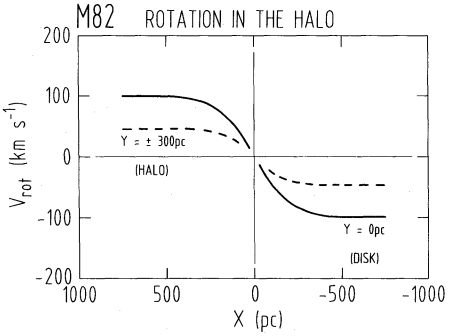

Fig. 11. Schematic rotation curves in M 82 which vary as a function of the height from the galactic plane. Note that the rotation in the halo is much slower than that in the disk

4.2. *Mass of the molecular gas*

For the optically thin case the column density N_{CO} of CO molecules can be determined from the relation

$$N_{CO}[\mathrm{cm}^{-2}] \simeq 0.3\ 10^{14}\ Q \int T_b\ dv\ [\mathrm{K\,km\,s}^{-1}], \quad (4)$$

where $Q \sim 5$ is the partition function for $T_{ex} \sim 20$ K and $T_b \sim T_R^*$ is the brightness temperature. We here adopt the main beam brightness temperature $T_{mb} \equiv T_R^*/\eta_{c,mb}$ for T_b, where $\eta_{c,mb}$ ($\simeq 0.63$) is the coupling efficiency of the main beam.

For the central positions of M 82 we obtain $\int T_b$ [CO (2−1)] $dv \sim 0.5\ 10^3$ K km s^{-1}, so that $N_{CO} \simeq 0.7\ 10^{17}$ [^{12}CO cm^{-2}]. However, in M 82 the CO (2−1) emission is not everywhere optically thin, and therefore the above estimate gives merely a lower limit to the molecular column density.

The H_2 mass was estimated integrating the profiles on the observed area. This integration gave

$$\sum_{ijk} T_{b_{ijk}}\, \Delta x_i\, \Delta y_j\, \Delta v_k = 2.4\ 10^{45}\ \mathrm{K\,km\,s}^{-1}\,\mathrm{cm}^2$$

Adopting the usually quoted value of $[CO]/[H_2] \sim 5\ 10^{-5}$ (e.g. Dickman, 1975), we obtain $M_{H_2} \sim 1.2\ 10^7\ M_\odot$. This result is consistent with the H_2 mass of $\sim 10^8\ M_\odot$ obtained for a wider area of 1400 pc × 1400 pc from the ^{12}CO ($J = 1-0$) observations of Nakai et al. (1987). The molecular mass obtained here shares about 10% of the dynamical mass of the same area as estimated from the rotation velocity.

4.3. *Galactic rotation in the halo*

A new, important aspect on the galactic dynamics can be derived from an inspection of the position (X)-velocity diagrams in Fig. 7. The $X-V$ diagrams obtained near the galactic plane (i.e. for $Y = 0'.0, \pm 0'.1$) show quite normal rotation for the disk and ring with a rotation velocity of $V_{rot} \sim 100$ km s^{-1} (Fig. 8). However, the rotation velocity clearly decreases as a function of the vertical distance from the galactic plane. In fact, the $X-V$ diagrams at $Y = \pm 0'.3$ can be well fitted by rotation with $V_{rot} = 50$ km s^{-1}. In Fig. 11 we schematically illustrate the variation of the rotation curves with height Y. The apparent slow rotation above the plane of M 82 can be interpreted in the following three ways:

(1) Slower rotation in the halo. The CO rotation velocity at $Y = \pm 0'.3$ is consistent with the 50 km s^{-1} rotation velocity of an extended diffuse Hα component observed by Bland and Tully (1988).

(2) Rotation of the near and far sides of the disk plane: With an inclination of 82° (equal to the optical disk inclination), the emission at $Y = 0'.3$ must come from the disk at 2 kpc distance from the centre. This seems unlikely, as we do not see any significant CO emission at $X = 2$ kpc (2′.2).

(3) Warped inner disk: The emission at $Y = \pm 0'.3$ where we see the slow rotation, must come from a region not farther than 0.5 kpc (0′.5 in X) from the centre. The warped disk would then be outlined by the lowest contour in the intensity map. This would imply that the inclination of the warped disk, whose radius is some 500 pc, is ~50°, and this again seems not likely compared with the intensity distribution of the inner 200 pc ring, which is consistent with an almost edge-on orientation.

Furthermore, the $X-V$ curves at $Y = \pm 0'.3$ show a concentration at $X = \pm 200$ pc. This is reasonably explained if they represent the rotation of halo gas which is in a cylinder, while (2) and (3) fail to explain this, Hence, we favour case (1) to explain the velocity gradient of the CO gas along the minor axis of M 82.

We emphaize that such a variation in the rotation curve in a galactic halo is clearly detected for the first time although this result was indicated by the observation of a slow Hα component (Bland and Tully, 1988). This was not only because of the present high-resolution and high-sensitivity line observations, but also due to the fact that the scale height of gas in M 82 is exceptionally large owing to ejection activity out of the disk plane.

The slower rotation in the halo may be reasonably attributed to the transfer of angular momentum from the internal region of the galaxy, if the observed gas has been supplied by an ejection or an outflowing wind from the centre. Since M 82 is a star bursting,

peculiar galaxy with a large amount of gas injected into its halo, the variation of rotation velocity detected here might be a phenomenon particular to this galaxy alone. Alternatively, such a variation might be a rather general tendency as a consequence of the three-dimensional rotation characteristics in spiral galaxies. More detailed observations of the dynamics of the halo gas are highly desired not only for the outer regions of M 82 but also for other edge-on galaxies.

Postscript. The recent paper by Phillips and Mampaso (1989, *Astron. Astrophys.* **218**, 24) described ^{12}CO (2−1) observations of M 82 with a 30″ beam. There is good agreement in the basic data. A thorough comparison of all the M 82 CO data is much needed.

Acknowledgements. The authors are indebted to Prof. E. Fürst, to Dr. D. Downes of IRAM and to Pico Veleta staff, in particular to Dr. C.J. Salter, for their kind help with the observations. This work was done as part of the international collaboration under the financial supports by the Japan Society of Promotion of Sciences, the Alexander von Humboldt-Stiftung, and the Max-Planck-Gesellschaft.

References

Axon, D.J., Taylor, K.: 1978, *Nature* **274**, 37
Bingham, R.G., McMullan, D., Pallister, W.S., White, C., Axon, D.J., Scarrott, S.M.: 1976, *Nature* **259**, 463
Bland, J., Tully, R.B.: 1988, *Nature* **334**, 43
Burbidge, E.M., Burbidge, G.R., Rubin, V.C.: 1964, *Astrophys. J.* **140**, 942
Carlstrom, J.E.: 1988, in *Galactic and Extragalactic Star Formation*, eds. R.E., Pudritz, M. Fich, NATO ASI Series, Reidel, Dordrecht, p. 571
Cottrell, G.A.: 1977, *Monthly Notices Roy. Astron. Soc.* **178**, 577
Dickman, R.L.: 1975, *Astrophys. J.* **202**, 50
Gottesman, S.T., Weliachew, L.: 1977, *Astrophys. J.* **211**, 47
Heckathorn, H.M.: 1972, *Astrophys. J.* **173**, 501
Holmberg, E.: 1950, *Medd Lunds Astron. Obs. Ser.* II **128**, 1
Klein, U., Wielebinski, R., Morsi, H.W.: 1988, *Astron. Astrophys.* **190**, 41
Kronberg, P.P., Biermann, P., Schwab, F.R.: 1985, *Astrophys. J.* **291**, 693
Kronberg, P.P., Pritchet, C.J., van den Bergh, S.: 1972, *Astrophys. J.* **173**, L47
Lo, K.Y., Cheung, K.W., Masson, C.R., Phillips, T.G., Scott, S.L., Woody, D.P.: 1987, *Astrophys. J.* **312**, 574
Loiseau, N., Nakai, N., Wielebinski, R., Sofue, Y., Klein, U.: 1988a, in *Molecular Clouds in the Milky Way and External Galaxies*, eds. R. Dickman, R. Snell, J. Young, Springer, Berlin, Heidelberg, New York, p. 407
Loiseau, N., Reuter, H.-P., Wielebinski, R., Klein, U.: 1988b. *Astron. Astrophys.* **200**, L1
Lugton, J.B., Watson, D.M., Crawford, M.K., Genzel, R.: 1986, *Astrophys. J.* **311**, L51
Lynds, C.R., Sandage, A.R.: 1963, *Astrophys. J.* **137**, 1005
Nakai, N., Hayashi, M., Handa, T., Sofue, Y., Hasegawa, T.: 1987, *Publ. Astron. Soc. Japan* **39**, 685
Nilson, P.: 1973, *Uppsala Astron. Obs. Ann.* **6**
O'Connell, R.W., Mangano, J.J.: 1978, *Astrophys. J.* **221**, 62
Olofsson, H., Rydbeck, G.: 1984, *Astron. Astrophys.* **136**, 17
Reich, W., Sofue, Y., Wielebinski, R., Seiradakis, J.H.: 1988, *Astron. Astrophys.* **191**, 303
Rickard, L.J., Palmer, P., Morris, M., Zuckerman, B., Turner, B.E.: 1975, *Astrophys. J.* **199**, L75
Rickard, L.J., Palmer, P., Morris, M., Turner, B.E., Zuckerman, B.: 1977, *Astrophys. J.* **213**, 673
Rieke, G.H., Lebofsky, M.J., Thompson, R.I., Low, F.J., Tokunaga, A.T.: 1980, *Astrophys. J.* **238**, 24
Sandage, A.R.: 1961, *The Hubble Atlas of Galaxies*, Carnegie Institution, Washington, p. 41
Schmidt, G.D., Angel, J.R.P., Cromwell, R.H.: 1976, *Astrophys. J.* **206**, 888
Seaquist, E.R., Bell, M.P., Bignell, R.C.: 1985, *Astrophys. J.* **294**, 546
Sofue, Y.: 1988, in *Galactic and Extragalactic Star Formation*, eds. R.E. Pudritz, M. Fich, NATO ASI Series, Reidel, Dordrecht, p. 409
Solomon, P.M., deZafra, R.: 1975, *Astrophys. J.* **199**, L79
Solomon, P.M., Scoville, N.Z., Sanders, D.B.: 1979, *Astrophys. J.* **232**, L89
Stark, A.A., Carlson, E.R.: 1984, *Astrophys. J.* **179**, 122
Stark, A.A., Wolff, R.S.: 1979, *Astrophys. J.* **229**, 118
Sutton, E.C., Masson, C.R., Phillips, T.G.: 1983, *Astrophys. J.* **275**, L49
Tammann, G.A., Sandage, A.R.: 1968, *Astrophys. J.* **151**, 825
Telesco, C.M., Harper, D.A.: 1980, *Astrophys. J.* **235**, 392
Vaucouleurs, G. de, Vaucouleurs, A.: 1964, *Reference Catalogue of Bright Galaxies*, University of Texas Press
Visvanathan, N., Sandage, A.R.: 1972, *Astrophys. J.* **176**, 57
Watson, M.G., Stanger, U., Griffiths, R.E.: 1984, *Astrophys. J.* **286**, 144
Weliachew, L., Fomalont, E.B., Greisen, E.W.: 1984, *Astron. Astrophys.* **137**, 335
Wunderlich, E., Klein, U., Wielebinski, R.: 1987, *Astron. Astrophys. Suppl.* **69**, 487
Young, J.S., Scoville, N.Z.: 1984, *Astrophys. J.* **187**, 153